Review

3 T MR tomography of the brachial plexus: Structural and microstructural evaluation

Ammar Mallouhi *, Wolfgang Marik, Daniela Prayer, Franz Kainberger, Gerd Bodner, Gregor Kasprian

Department of Radiology, Division of Neuroradiology and Musculoskeletal Radiology, Medical University of Vienna, Waehringer Guertel 18-20, A-1090 Vienna, Austria

ARTICLE INFO

ABSTRACT

Magnetic resonance (MR) neurography comprises an evolving group of techniques with the potential to allow optimal noninvasive evaluation of many abnormalities of the brachial plexus. MR neurography is clinically useful in the evaluation of suspected brachial plexus traumatic injuries, intrinsic and extrinsic tumors, and post-radiogenic inflammation, and can be particularly beneficial in pediatric patients with obstetric trauma to the brachial plexus. The most common MR neurographic techniques for displaying the brachial plexus can be divided into two categories: structural MR neurography; and microstructural MR neurography. Structural MR neurography uses mainly the STIR sequence to image the nerves of the brachial plexus, can be performed in 2D or 3D mode, and the 2D sequence can be repeated in different planes. Microstructural MR neurography depends on the diffusion tensor imaging that provides quantitative information about the degree and direction of water diffusion within the nerves of the brachial plexus, as well as on tractography to visualize the white matter tracts and to characterize their integrity. The successful evaluation of the brachial plexus requires the implementation of appropriate techniques and familiarity with the pathologies that might involve the brachial plexus.

1. Introduction

Since its introduction in 1992 [1], MR neurography has gained greater acceptance as an important diagnostic adjunct to the clinical evaluation of patients with lesions of the brachial plexus [2,3]. In addition, because of its non-invasive nature and its ability to evaluate the proximal and distal parts of the brachial plexus, MR neurography has replaced CT myelography, which has long been used in the assessment of preganglionic root injuries. State-of-the-art MRI is becoming the primary imaging modality for morphological depiction of the brachial plexus and characterization of its pathological conditions [4–6]. The main purpose of MR imaging is to determine whether a particular pathology is present in the brachial plexus, and also to characterize the location and extent of such pathology. In order to successfully achieve this objective, the MR examination should enable a clear structural analysis of the brachial plexus, from its origin at the cervical spinal cord to its terminal branches, as well as provide a picture of the surrounding tissues and help to determine intraneural functional integrity.

In this article, we review the basic concepts of brachial plexus imaging and describe the key elements in the structural and microstructural evaluation of the brachial plexus by illustrating potential clinical applications for MR neurography with regard to traumatic injuries, neoplastic abnormalities, thoracic outlet syndrome and postoperative follow-up.

2. MR anatomy of the brachial plexus

MR tomographic analysis of the brachial plexus is considerably facilitated by a thorough knowledge of its anatomy and the recognition of particular anatomical landmarks, i.e., the fist rib and clavicle, the subclavian artery and vein, as well as the anterior and middle scalene muscles. The brachial plexus, formed in the majority of individuals from the ventral rami of C5 to T1, with or without minor branches from C4 and T2, supplies the upper extremity with motor and sensory function [7]. A lesion or damage to a part of these neural structures often produces a clear loss of function of an upper extremity.

The brachial plexus is divided into five segments: roots; trunks; divisions; cords; and terminal branches (Fig. 1). After exiting the neural foramen of the cervical spine, the roots of the brachial plexus pass through the interscalene triangle, an anatomical structure that is formed anteriorly by the anterior scalene muscle and posteriorly by the middle scalene muscle and which also houses the subclavian artery in its inferior section. The roots then combine in the

* Corresponding author. Tel.: +43 1 40400 4895; fax: +43 1 40400 4555.
E-mail addresses: Ammar.Mallouhi@meduniwien.ac.at (A. Mallouhi),
Wolfgang.Marik@meduniwien.ac.at (W. Marik), Daniela.Prayer@meduniwien.ac.at
(D. Prayer), Franz.Kainberger@meduniwien.ac.at (F. Kainberger),
Gerd.Bodner@meduniwien.ac.at (G. Bodner), Gregor.Kasprian@meduniwien.ac.at
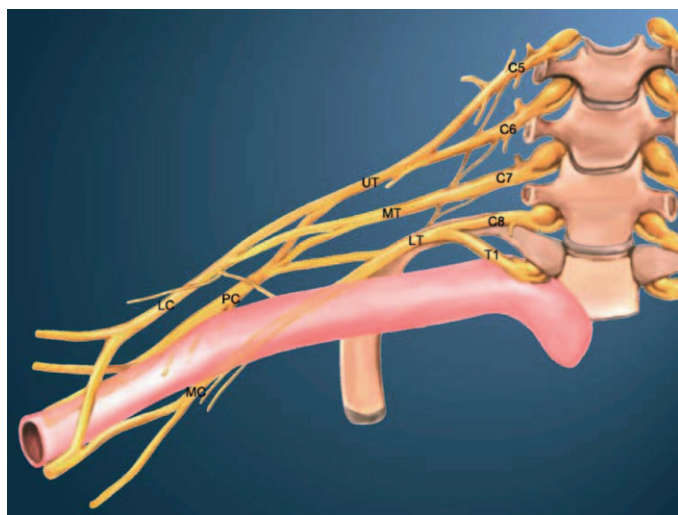(G. Kasprian).

Fig. 1. A diagram demonstrating the five segments of the brachial plexus, i.e., roots (C5 to T1), trunks (upper trunk, UT; middle trunk, MT; and lower trunk, LT), divisions, cords (lateral, LC; posterior, PC; and medial, MC) and terminal branches.

lateral part of the interscalene triangle to form three trunks: the upper trunk, formed from the union of the C5 and C6 roots; the middle trunk, formed solely from the C7 root; and the lower trunk, formed from the union of C8 and T1. Each trunk provides an anterior and a posterior division. The divisions reunite to form the lateral, posterior, and medial cords that are named according to their relationship to the adjacent subclavian artery. The cords pass through the costoclavicular space, an anatomical structure located between the clavicle superiorly and the first rib inferoposteriorly. The cords divide into the terminal branches. The main branches of the lateral cord are the musculocutaneous nerve and the lateral root of the median nerve. The branches of the medial cord are the ulnar nerve and the medial root of the median nerve, and those of the posterior cord are the radial nerve and the axillary nerve.

3. MR neurography of the brachial plexus

3.1. Protocol concept

Brachial plexopathies are challenging diagnostic problems that require careful selection of MR sequences and proper anatomical adjustment to cover the entire region of the brachial plexus in the representative planes. With the rapid pace of developments in this field of MR imaging, protocols are constantly evolving, and a specific protocol as the only approach to a comprehensive MR neurographic examination of the brachial plexus cannot be proposed. Rather, an appropriate combination of MR sequences, such as shown in Tables 1 and 2, should be assembled according to the clinical indication of the examination, the technology available and the personal justification of the responsible radiologist. Such an examination protocol yields different types of information that, together, can be helpful in establishing the correct diagnosis.

A comprehensive MR protocol for the brachial plexus can be developed to facilitate evaluation of the morphology of brachial plexus nerve structures and to help in obtaining information about intraneural integrity; the former by using conventional MRI sequences (fat saturated T2-weighted sequences for imaging extradural plexus components and MR myelography sequences for imaging intradural nerve rootlets) and the latter by using diffusion tensor imaging with tractography, which allows a noninvasive characterization of tissue structure, by measuring the degree and directionality of proton motion. Depending on the indication, the assessment of the surrounding tissues of the brachial

plexus requires T1- and T2-weighted sequences, which also further serve in the evaluation of signal intensity characteristics and detection of pathologic contrast enhancement of the neural structures of the brachial plexus.

The injection of gadolinium is necessary in infectious, inflammatory, neoplastic, and post-radiogenic disorders of the brachial plexus or its surrounding tissues, as well as in postoperative cases. In posttraumatic injuries, the application of gadolinium in the acute phase is not necessary, while in chronic plexopathies, gadolinium may reveal scar tissue. For the evaluation of plexopathies of undefined character, the application of gadolinium depends on the findings on nonenhanced images, but gadolinium application may reveal harbored lesions.

As important as the selection of the appropriate sequences for examining the brachial plexus is achieving adequate anatomical coverage with proper signal gain to ensure a successful examination. The entire brachial plexus should be imaged and a correspondingly wide FOV is a prerequisite despite the high in-plane resolution of the applied sequences. Therefore, the selection of a suitable coil that covers the brachial plexus from the spinal cord to the axilla is a key element. The use of an 8- or 16-channel neurovascular coil enables the examination of the entire brachial plexus. With its 18 elements that could be individually activated, the neurovascular coil provides a large area of coverage from the top of the head to the aortic arch, including both shoulder regions. A neurovascular coil can be used in addition to examining the brachial plexus for imaging the brain, the pituitary gland, the internal acoustic canal, the cerebral and cervical arteries, and the cervical spine.

Also helpful in the examination of the brachial plexus is the use of parallel imaging or coil sensitivity encoding (Sense). The Sense technique uses the simultaneous information from all coil elements and the knowledge of the spatial sensitivity variation of each coil element to reconstruct the full image [8]. The faster acquisition obtained with SENSE could be translated directly into shorter scanning, which leads to a shorter total exam time and a decrease in motion artifacts. Another application for Sense is to use the rapid acquisition to enhance resolution or to increase the number of slices. Further, a contrast improvement can be obtained with Sense in sequences with transient behavior, such as inversion recovery sequences. In the period when the background signal crosses zero, more data can be obtained with Sense, resulting in better background suppression [8]. For the acquisition of diffusion tensor images, the reduction of the echo time due to parallel imaging minimizes magnetic susceptibility artifacts and distortions. Further, the SENSE acquisition accomplished a significant increase in SNR efficiency leading to high-resolution tensor mapping.

Furthermore, cardiac or respiratory gating is useful to minimize motion artifacts. However, these techniques extend the acquisition time considerably, and consequently, the overall examination time that mounts already up to 40–60 min. In general practice, the quality of non-gated images is adequate for diagnosis.

3.2. MR neurography at 3 T

Satisfactory MR neurograms of the brachial plexus can be obtained at either 1.5 T or 3 T. Several articles have described the imaging characteristics of the brachial plexus using a 1.5 T MR scanner [2,5,6], which was preferred by some investigators [4] for brachial plexus imaging. However, other investigators [9,10], including us, basically prefer to benefit from the higher field strength at 3 T MR imaging for the evaluation of brachial plexopathies.

The primary benefit of imaging at high field strength is the increased SNR. This is a direct consequence of the increase in MR signal that results from the greater number of protons aligned with the main magnetic field [11]. Compared to 1.5 T, using 3 T permits

Table 1
2D sequences for MR imaging of the brachial plexus.

2D sequences	Orientation	FOV, mm	Slice Thickness, mm	Slice gap, mm	TR, ms	TE, ms	Flip angle	Acquisition duration, min	Number of slices	Voxel size, mm
T2W-STIR	Coronal	270	2.7	0.3	3000	60	90°	5:50	17	0.8 × 0.8 × 2.7
T2W-STIR	Coronal	350	3.5	0.3	6780	60	90°	3:50	27	1 × 1.4 × 3.5
T2W-STIR	Sagittal	255	3	0.3	2500	60	90°	4:00	17	0.9 × 1.2 × 3
T2W-STIR	Axial	320	4	0.4	9760	60	90°	4:33	40	1 × 1.4 × 4
T2W-TSE	Sagittal	250	3	0.3	3000	80	90°	2:50	14	0.5 × 0.75 × 3
T2W-TSE	Axial	330	3	0.3	7090	75	90°	3:05	30	1 × 1 × 3
T2W-BFFE	Axial	225	5	-2.5	8	3.7	45°	2:15	30	0.7 × 0.7 × 5
T1W-SE	Coronal	250	4	0	500	18	90°	5:10	21	0.8 × 1 × 4
T1W-TSE + FS	Coronal	250	4	0	500	18	90°	5:10	21	0.8 × 1 × 4
T1W-SE	Axial	300	3	0.3	530	14	90°	3:10	22	1 × 1 × 3
T1W-TSE + FS	Axial	300	3	0.3	530	14	90°	3:10	22	1 × 1 × 3

a 4-fold increase in signal, as well as a 2-fold increase in noise, and therefore, SNR should increase 2-fold at 3 T. However, because of certain limitations of 3 T MR imaging, including alterations in relaxation times and in total body heating, the realized gain in SNR over that at 1.5 T is usually 1.7- to 1.8-fold [11]. The higher SNR can be exploited, within a particular examination, in two different ways, either to increase the spatial resolution, or indirectly, to decrease the acquisition time. This increased spatial resolution at axial (in-plane) imaging has the potential to improve lesion visibility. The finer detail on reformatted (through-plane) images may aid in lesion characterization [11]. A further advantage of 3 T MR imaging is that image contrast can be improved by applying contrast media, such as gadolinium. Although T1 usually increases at 3 T imaging, even with the use of gadolinium, gadolinium-enhanced tissues stand out markedly against the background because the T1 of gadolinium is shorter than that of the soft tissues. This improvement in contrast provides an opportunity for gadolinium dose reduction.

A further advantage of 3 T imaging is its feasibility in the application of diffusion tensor fiber tractography. One of the major limitations of diffusion tensor imaging is its limited spatial resolution (voxel volume). Improving the spatial resolution is crucial for fiber tractography. Although the MR sequence typically used for the acquisition of diffusion tensor imaging, i.e., echo planar imaging, allows rapid acquisitions, it is necessary to reduce the echo time to improve the spatial resolution or to increase the power of gradients and magnetic field. The improvement in SNR at 3 T compared to 1.5 T enables the reconstruction of highly resolved DTI parametrical maps, with enhanced depiction of the fiber tracts and better concordance with the expected anatomy of the spinal cord and the brain [12].

The disadvantages of 3 T imaging include RF Field inhomogeneity, which increases with greater field strength. At higher field strengths, the magnetic field is more inhomogeneous and more sensitive to T2* dephasing characteristics. Further, T2 may slightly decrease with increasing magnetic field strengths. This would further reduce the SNR gain for the long TE sequences required for the imaging of the brachial plexus. In addition, the SAR increases with the square of the resonance frequency, and, therefore, the square of the magnetic field [11].

With regard to MR imaging of the brachial plexus in particular, the visibility of its trunks and cords has been reported to be objectively and subjectively superior at 3 T than at 1.5 T in volunteers as well as in patients [9]. Objectively, the SNR of the brachial plexus nerves increases significantly at 3 T, especially for T2-weighted TSE sequence with fat saturation. Specifically, the SNR of the plexus nerves increases approximately three times that of 1.5 T at 3 T. The CNR between muscle and nerve for T1-weighted TSE and for T2-weighted TSE with fat saturation also increases 1.5–2 times at 3 T compared with 1.5 T MR imaging. Subjectively, the visibility of the brachial plexus and its anatomical parts at 3 T appears to be superior to that at 1.5 T. Further, artifacts on T2-weighted TSE with fat saturation at 3 T seem less relevant than on 1.5 T, while there are no significant differences regarding artifacts on T1-weighted TSE images at 1.5 T and 3 T.

4. Structural evaluation of the brachial plexus

4.1. Imaging sequences

Although the anatomy and morphology of proximal nerve segments of the brachial plexus can be well-analyzed on T1-weighted sequences, the T2 STIR (short term inversion recovery) sequence seems to be the best MRI technique for the evaluation of peripheral nerve disorders. This is because it provides a homogeneous fat saturated image with excellent T2-weighted contrast, resulting in accentuated delineation of the neural plexus segments that can be optimally distinguished from the surrounding fat tissues (Figs. 2–6). The nerves appear considerably hyperintense within a hypointense fat saturated background on STIR images, and therefore, the STIR sequence is usually considered as MR neurography. To enhance the contrast between the brachial plexus and its surroundings, an inversion recovery magnetization preparation, with TI = 180 ms for fat saturation, can be included in the acquisition of

Table 2
3D sequences for MR imaging of the brachial plexus.

| 3D sequences	Orientation	FOV, mm	Slice thickness, mm	Slice gap, mm	TR, ms	TE, ms	Flip angle	Acquisition duration, min	Number of slices	Voxel size, mm
DTI	Sagittal	196	4	0	2000	101	90°	6:24	22	2.5 × 2.5 × 4
DTI	Axial	375	4	1	3000	90	90°	6:30	50	4 × 4 × 4
T2W-STIR	Coronal	350	0.9	0	4000	218	90°	8:24	112	0.9 × 0.9 × 0.9
T2W-BTFE	Sagittal	200	1	−0.5	6.2	3.1	60°	7:00	86	0.6 × 0.6 × 1
T2W-TSE	Axial	180	1	−0.5	2000	240	90°	8:40	95	0.7 × 0.9 × 1
3D CISS	Axial	180	1.4	−0.7	2000	130	90°	6:40	80	0.7 × 0.9 × 1.4
T1W-THRIVE	Axial	360	1	0	8.1	3.7	7°	2:55	120	1 × 1 × 1
T1W-VIBE	Coronal	450	2	0.4	2.78	1.0	13°	0:22	88	2.3 × 1.8 × 2
T1W-VIBE	Axial	350	2	0.4	2.78	1.0	13°	0:18	88	1.8 × 1.4 × 2
T1W MP-Rage	Coronal	375	1	0.5	1950	2.3	9°	6:53	120	1 × 1 × 1
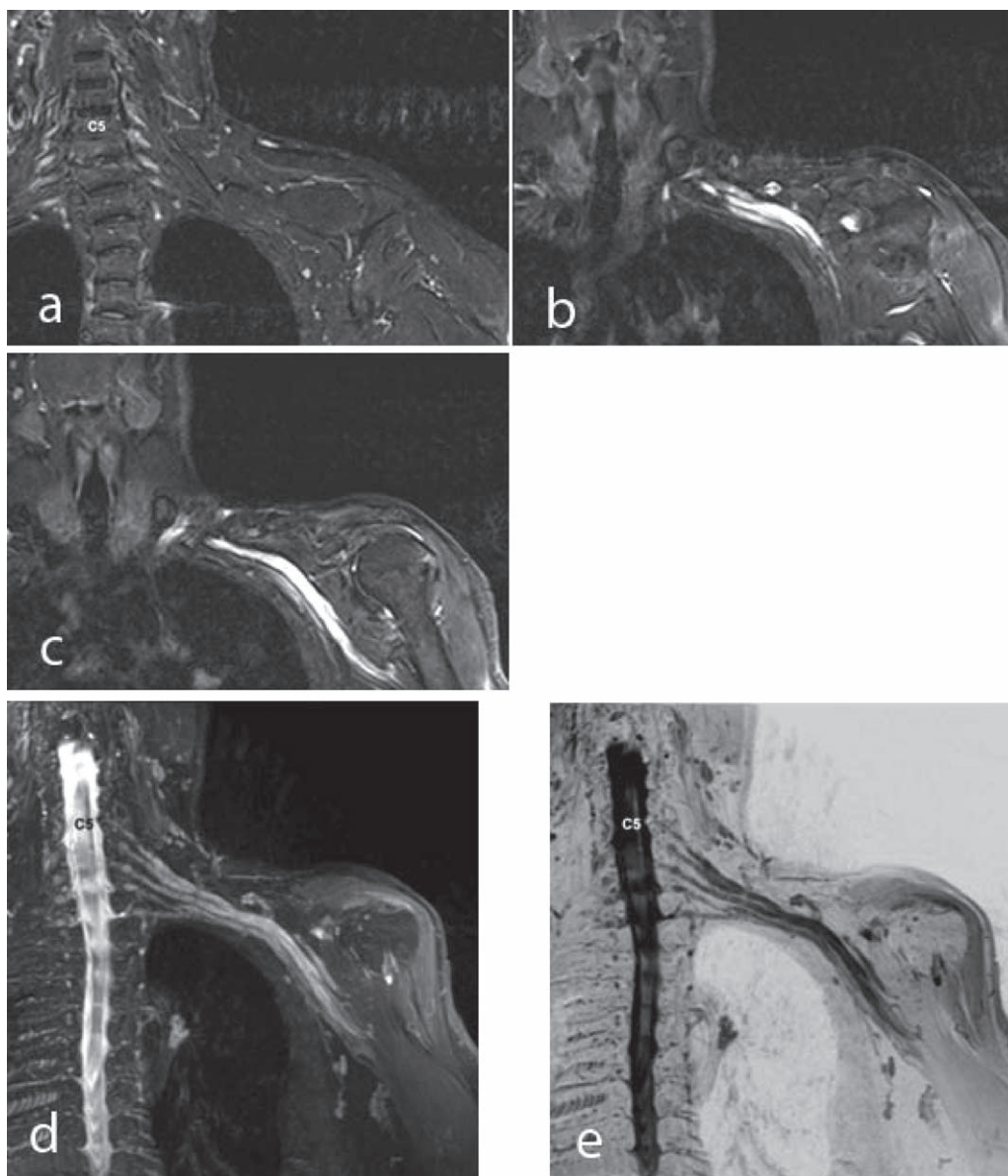
Fig. 2. Serial coronal 2D STIR images (a) show only parts of the roots, trunks (b) and cords (c) of the brachial plexus in a patient with trauma to the left shoulder and a considerable swelling and signal increase in the middle trunk and the lateral cord. The MIP image (d) and the inverted MIP image (e) show the entire brachial plexus with diagnostic details.

STIR. The STIR sequence is also beneficial for the detection of neo-plastic involvement of the adjacent bony structures, and for the presence of lymphadenopathy, edema and soft tissue infiltration. Traditionally, 2D T2 STIR is used in the evaluation of the brachial plexus, but, recently, the use of 3D STIR was reported to be feasible [4,5]. The main advantage of 3D T2 STIR is the high resolution and complete coverage of the brachial plexus, which can then be evaluated in any arbitrary plane, as required. The shorter acquisition time and the enhanced contrast between the brachial plexus and its surrounding tissues are the main advantages of 2D T2 STIR, and therefore, seems to have an advantage in examining patients with acute injuries of the brachial plexus. Further, with 2D STIR, images can be performed with a wide FOV that includes both shoulders to compare the pathologic side with the normal one and to better recognize muscle atrophy and joint deformities.

In general, T2 STIR images are not suitable for the evaluation of intradural nerve rootlets. For this purpose, MR myelography, which uses balanced, steady-state free precession sequences such as fast imaging with steady state precession (True-FISP), fast imaging employing steady state acquisition (FIESTA), the balanced turbo field echo (BTFE), the balanced fast field echo (BFFE), three-dimensional T2-weighted TSE and constructive inter-ference in steady state (3D CISS), plays an important role. Because of the high spatial resolution, strong T2 contrast, high SNR, and inherent flow compensation, MR myelography sequences provide a diagnostic visualization of structural abnor-malities of the intradural nerve rootlets, as well as of the thecal sac (Fig. 7a and b). However, MR myelography sequences have some limitations, including the long acquisition times and CSF pulsation artifacts, which are more pronounced at higher field strengths, and, consequently, may impair, to var-ious degrees, the delineation of the intradural nerve rootlets (Fig. 7c).

T1-weighted images may be obtained either in 2D, i.e., by using spin echo sequences, or in 3D, i.e., by using the T1-MPR or T1 high-resolution isotropic volume excitation (THRIVE) sequences. Both
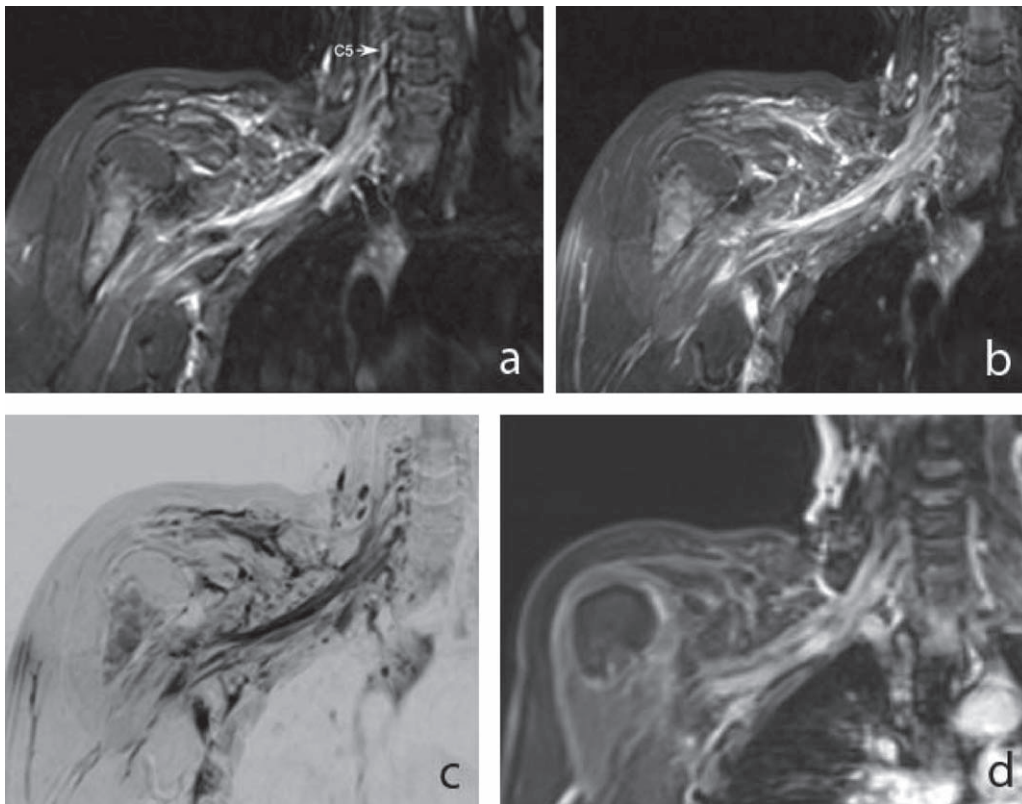
Fig. 3. Paracoronal 2D STIR image (a) in a patient with radiation therapy to the right shoulder shows diffuse thickening and a signal increase in the partially demonstrated brachial plexus as well as a signal increase in the surrounding fat tissues. The MIP image (b) and the inverted MIP image (c) present a more comprehensive view of the radiation-induced brachial plexopathy, with a typical enhancement pattern, as seen on the reconstructed MIP image of THRIVE sequence (d).

2D and 3D T1-weighted images are more helpful when applied with fat saturation after gadolinium injection (Figs. 3d and 5c).

4.2. Imaging planes

When using 2D sequences, particularly the T2 STIR sequence, the orientation of these sequences plays an important role in providing adequate anatomical coverage of the brachial plexus. The individual spinal nerves serve as a lead in planning the sequence planes. The most important plane for imaging the brachial plexus is the coronal plane, i.e., either a strict coronal (parallel to the spinal canal long axis on the sagittal plane), or a paracoronal (parallel to the spinal canal long axis on the sagittal plane and simultaneously to the brachial plexus long axis on the axial plane). The advantage of the coronal plane is the symmetric demonstration of the anatomical structures in a well-known perspective; however, the coronal planes depict only a small part of the brachial plexus on each image (Fig. 2) and the evaluation of the brachial plexus requires viewing several consecutive coronal images. In contrast, paracoronal images provide an oblique and less familiar perspective of the anatomical structures, but they depict a large part of the brachial plexus on one paracoronal image (Fig. 3).

Although less useful than the coronal plane, the axial plane also enables a good diagnostic presentation of the entire brachial plexus, both in the strict axial plane (Fig. 4a) as well as in an oblique paraxial plane (Fig. 4b). The sagittal plane provides a good perspective of the anatomical muscular (the anterior and middle scalene muscles), vascular (subclavian artery and vein), and osseous (the fist rib and clavicle) landmarks surrounding the brachial plexus. Further, the sagittal plane can be used to identify the nerve root exits and the course of the plexus structures (Fig. 5). Usually, applying the T2 STIR sequence in two planes is adequate for a diagnostic result.

4.3. Image postprocessing

Applying postprocessing techniques, such as slab MIP and multiplanar reformation to 3D sequences, such as 3D STIR, FIESTA, and THRIVE in brachial plexus MR imaging, enables an interactive evaluation and an arbitrary perspective of the imaged region. Thus, these techniques assist in the recognition and characterization of plexus lesions. Postprocessing techniques for 2D sequences are not essentially required to reach a diagnosis, and, because of their lower spatial resolution compared to 3D sequences, the feasibility of slab MIP and multiplanar reformation on 2D sequences is limited. However, when using 3 T MR imaging techniques, it is possible to reconstruct slab MIP images (Fig. 2d) and multiplanar reformation of 2D STIR images with adequate diagnostic quality, and with the ability for interactive evaluation in oblique planes. Slab MIP, particularly when performed with up to 50% overlapping, enables the demonstration of the plexus nerves from their origin to their periphery on one to two images (Figs. 2d, 3b, and 5b,c). In addition, MIP assists in improving the delineation of the plexus nerves against the surrounding fat-suppressed tissues. A further postprocessing technique that may be visually helpful is the gray scale inversion technique for MIP images (Figs. 2e and 3c). The latter technique may improve the delineation of the plexus segments, but provides no more information than that already depicted on conventional MIP images.

4.4. Clinical practice

4.4.1. Trauma

The main indication for brachial plexus MR imaging in adults is the traumatic injury. The most common cause of traumatic plexus injury is high-velocity trauma, such as motorcycle accidents due
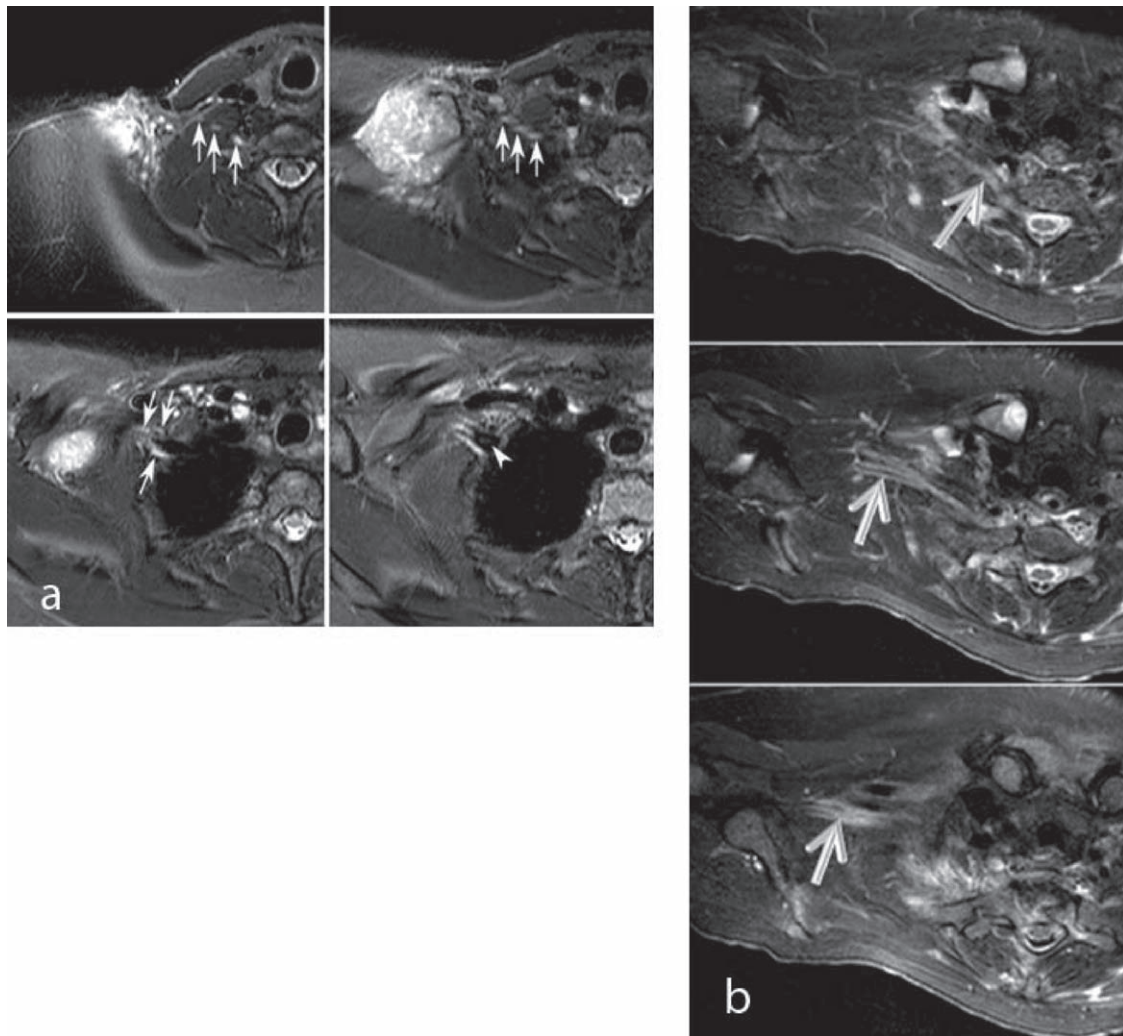
Fig. 4. Serial axial 2D STIR images (a) in a patient with a supraclavicular soft tissue metastasis show the nerves (arrows) of the brachial plexus passing nearby the tumor. Serial paraaxial 2D STIR images (b) in a different patient with multiple soft tissue and osseous metastases in the neck and both shoulders provide a diagnostic view of the intact nerves (arrows) of the brachial plexus.

to stretching, bruising, or tearing plexus components. The purpose of MR imaging in this case is the detection and characterization of a plexus injury. Such an injury may range in the acute and subacute phase from a swelling (Fig. 2), to the disruption and retraction of plexus components, including hemorrhage, compression, and displacement. In the chronic phase, MRI helps in the detection of post-traumatic focal or diffuse fibrosis and neuromas that are usually caused by regenerating nerve fibers. A main element in the diagnosis is the recognition of the site of the injury, and, particularly in the case of plexus rupture, it is important to differentiate preganglionic from postganglionic injuries, since the latter can be surgically treated while the former has an unfavorable prognosis because restoration of continuity is not a surgical option. Through the direct inspection of nerve rootlets on MR myelographic images (Fig. 7a and b), a preganglionic rupture can be diagnosed or ruled out. An indirect indication of a preganglionic plexus injury is the presence of a pseudomeningocele, which is caused by a tear in the dural sac that forms a cyst-like deformation in the neural foramen (Fig. 7c). A pseudomeningocele is a common finding after nerve root avulsion, but can also be present with intact nerve roots.

4.4.2. Obstetric plexopathy

A special indication for brachial plexus MR imaging is the evaluation of obstetric plexus lesions usually caused by a traction injury during birth. This can lead to a rupture of C5 and C6 (Erb's palsy) and/or C7 and C8 (Klumpke palsy). Due to the need for sedation, the difficult logistic effort, and the small dimensions of the newborn's brachial plexus requiring a dedicated optimized protocol, MR imaging of obstetric plexus lesions is not widely available. Furthermore, the true clinical benefit of MRI in this condition is unclear, since the indication for surgical therapy is mainly based on clinical findings. In order to assess the value of early MR imaging to support the clinical decision between conservative or surgical therapy, this method must be included in future standardized clinical trials. The role of MR imaging of a newborn's brachial plexus would be both the detection of neural abnormalities, i.e., the presence of plexus disruption or a neuroma-in-continuity (Fig. 6) and the presence of musculoskeletal deformities, i.e., the recognition of shoulder muscle atrophy and glenohumeral joint deformity.

4.4.3. Tumors

A further important indication for brachial plexus MR imaging is the evaluation of intrinsic and extrinsic neoplastic abnormalities. The most common primary tumors are benign, and range between the more frequently seen schwannoma and solitary or neurofibromatosis I-associated neurofibroma, and the rarely seen lipoma, lymphangioma, neurofibrosarcoma, and desmoid tumors. Another type of intrinsic brachial plexus mass is the malignant peripheral
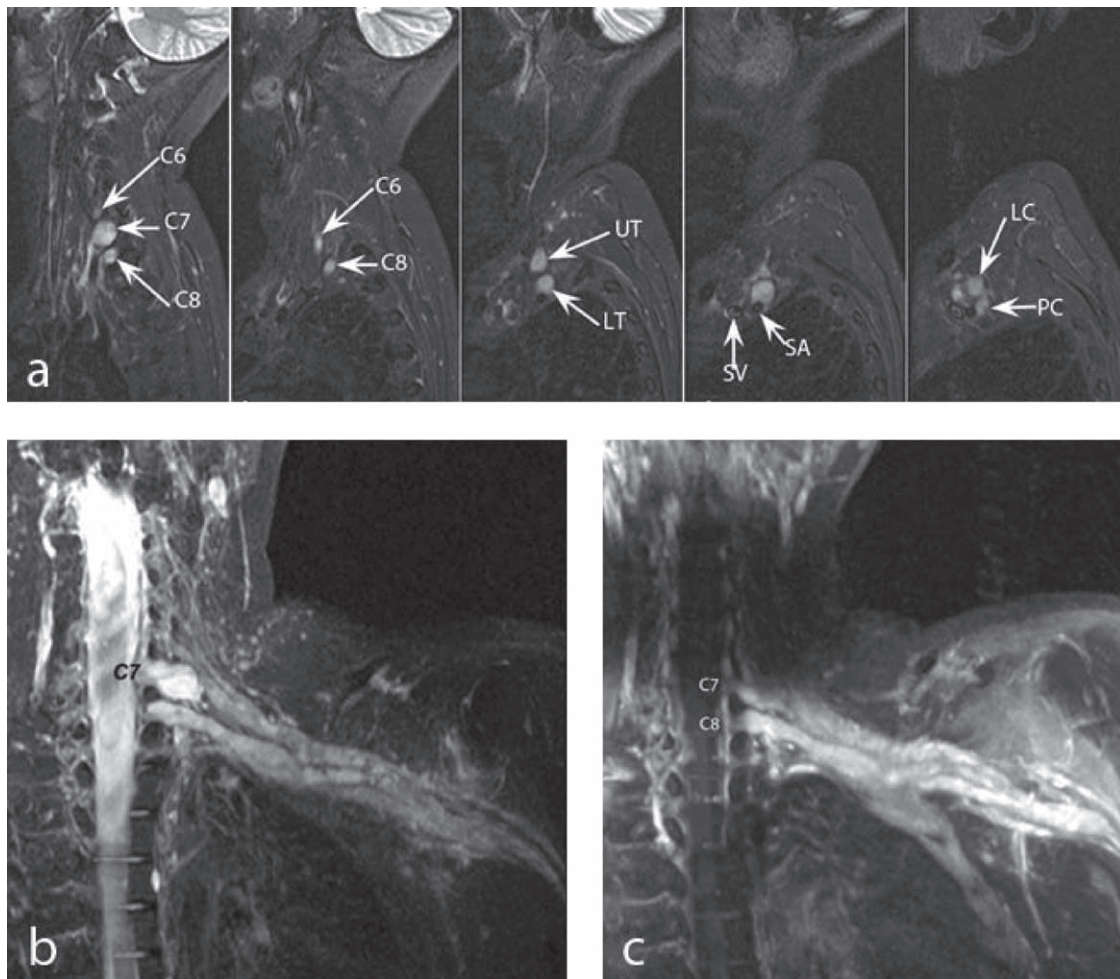
Fig. 5. Serial sagittal 2D STIR images (a) and paracoronal MIP image reconstructed from paracoronal 2D STIR images (b) in a patient with a malignant peripheral nerve sheath tumor of C7 that was resected and treated with radiotherapy. This follow-up examination shows multifocal thickening of several parts of the brachial plexus, especially C6 and C8, with severe contrast enhancement, as seen on the reconstructed MIP image of the THRIVE sequence (c), indicative of neoplastic plexopathy.

nerve sheath tumor, which appears rarely as a primary neoplasm, but more frequently as secondary to neurofibromatosis I, and after brachial plexus irradiation while treating a mediastinal, lung, or breast tumor, or a lymphoma. Plexus irradiation may also cause radiogenic plexopathy.

The differentiation between a radiogenic and a neoplastic plexopathy could pose a diagnostic dilemma. However, MR imaging provides important morphologic signs that favor one diagnosis over the other. In radiogenic plexopathy, caused usually by plexus fibrosis about one year after radiation, MRI shows morphologic
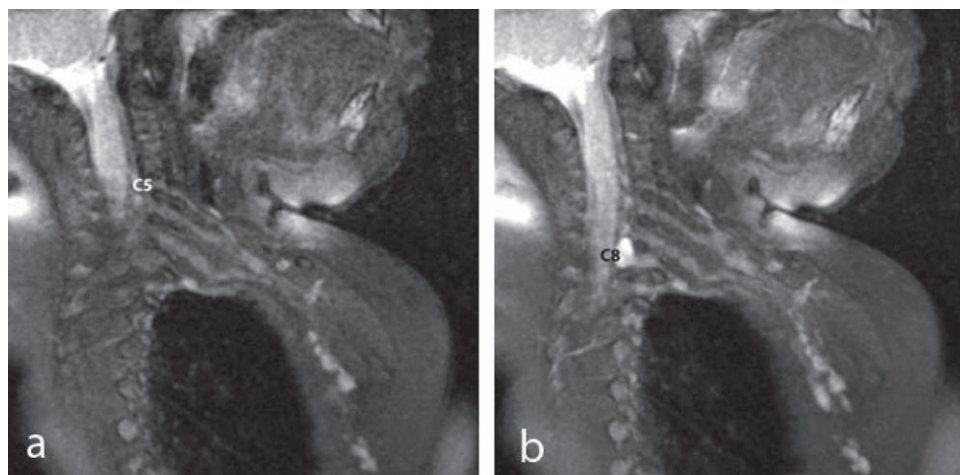

Fig. 6. Paracoronal 2D T2 STIR (a) in a 3-month-old girl with a brachial plexus birth injury shows a neuroma-in-continuity of the upper trunk. (b) Thin MIP image (acquired from the paracoronal 2D T2 STIR images) gives a better overview of the neuroma-in-continuity of the upper trunk and reveals a traumatic meningocele of C8.
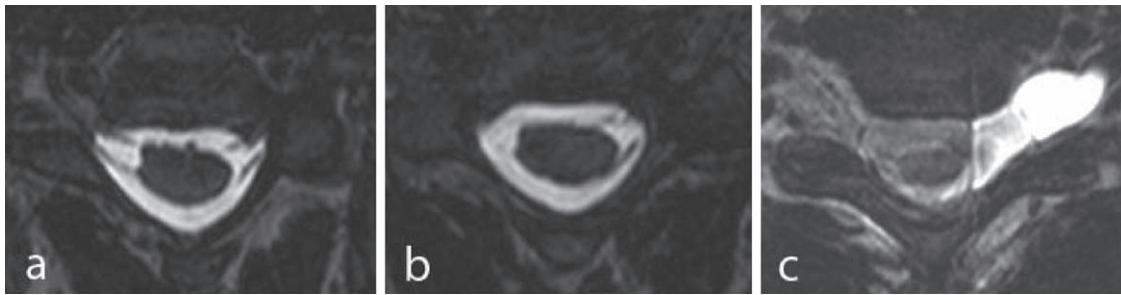
Fig. 7. Axial MR myelography at 3 T with thin-slab MIP in different patients. (a) Demonstrates normal rootlets of C6 with homogeneous signal intensity of the surrounding spinal fluid. (b) Shows normal left rootlets of C7, while the right rootlets of C7 are missing indicative of nerve root avulsion. (c) Normal right rootlets of C8, on the right side, with inhomogeneous signal intensity of the surrounding spinal fluid, but the image quality is adequate. On the left side, a considerable pseudomeningocele is present, while the left rootlets are not depicted, indicating nerve root avulsion.

changes involving the brachial plexus and its surrounding fat tissue and muscles (Fig. 3). The main sign is a diffuse and uniform thickening of the involved brachial plexus segments, with slight to moderate signal increase on STIR images and slight to moderate contrast material enhancement. Similarly, the surrounding fat tissues and muscles appear diffusely T2-hyperintense with diffuse contrast material enhancement. In addition, radiogenic pneumonia and pleura thickening might be seen at the lung apex. At the chronic stage, radiation fibrosis of the plexus appears usually with low signal intensity on T1- and T2-weighted images without contrast enhancement.

The main characteristic feature of a neoplastic plexopathy is a focal or multifocal thickening of a section of the plexus, mainly with a T2 signal increase and moderate to severe contrast material enhancement (Fig. 5). MR imaging might reveal, in such cases, metastatic lesions and lymph nodes. Nevertheless, differentiation between radiogenic and neoplastic plexopathy might require an MRI follow-up, FDG PET, or a combination of both.

Extrinsic neoplasms that involve the brachial plexus extend from the adjacent anatomical regions. The most common tumor that infiltrates the brachial plexus is the superior sulcus tumor,

i.e., the Pancoast tumor, which is a non-small cell lung carcinoma that arises from the lung apex and invades the thoracic inlet with involvement of the brachial plexus and may also infiltrate the neuroforamina, intraspinal space, vertebral bodies and subclavian vessels. Metastatic disease of the adjacent soft tissues and bones may also infiltrate the brachial plexus.

Fig. 9. Paracoronal 2D STIR image (a) in a patient with brachial plexus trauma, revealing a severe soft tissue edema around the plexus nerves, which seem to be swollen, with ill-defined caudal roots. 3D tractogram (b) shows the intact and continuous fibers of the C5 to C8 roots. No fibers could be detected on T1 sequences.

Fig. 8. Paracoronal 2D T2 STIR (a) in a patient with thoracic outlet syndrome, showing an elongated transverse process of C7 (large arrow) that displaces and presses the nerve root (small arrows). During the acquisition of this image, the left hand of the patient was placed on the right side of patient's abdomen rather than in the neutral position (beside the body).
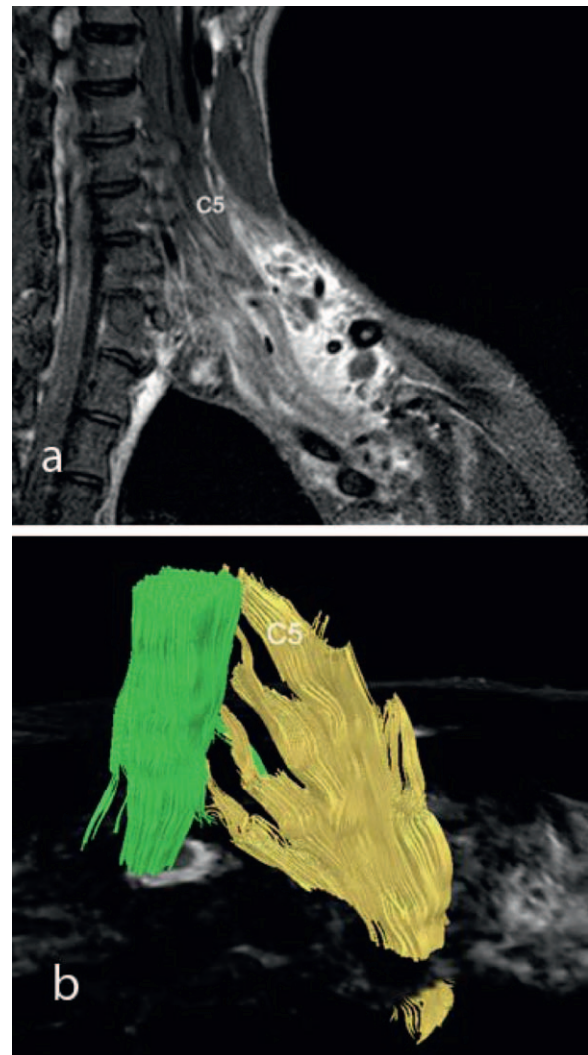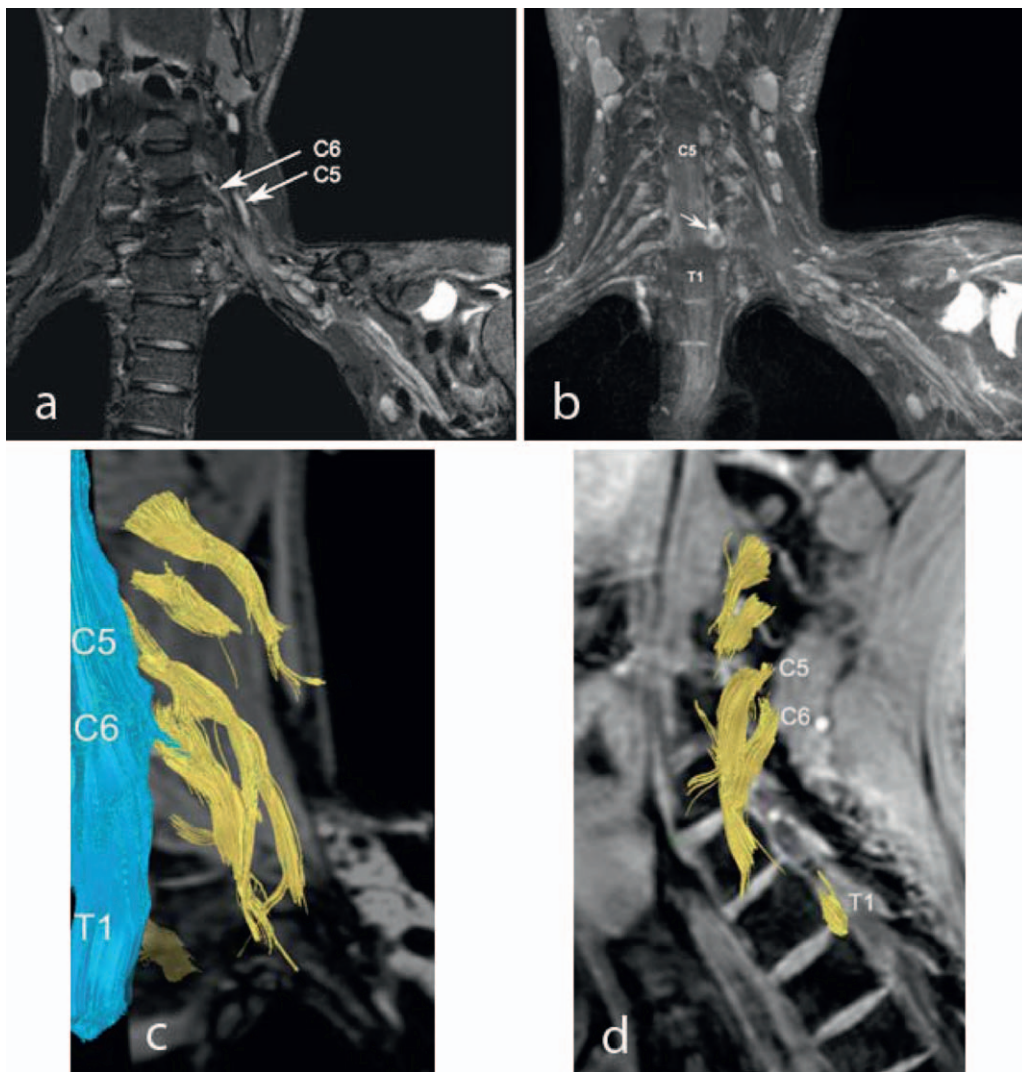
Fig. 10. Multi-segmental root abnormalities in a patient with traumatic brachial plexus injury. (a) Paracoronal 2D T2 STIR and (b) thin MIP image (acquired from the paracoronal 2D T2 STIR images) show disconnection of all five roots of the brachial plexus, with contraction and edematous thickening of the plexus cords (arrowheads). The MIP image (b) gives a good overview of the extent of the injury on the left side, revealing the presence of a traumatic meningocele and the normal morphology of the plexus on the right side. (c) Paracoronal and (d) sagittal 3D tractogramms that show persisting fibers in the C5, C6 and T1 roots, and in the proximal part of upper trunk, while no fibers were detected in C7 and C8 due to root avulsion. In addition, the nerve trunks inferior and lateral to the clavicle are clearly retracted. The impact of these tractograms is that they give the impression of a root avulsion of C8 (already suggested by the traumatic meningocele) and also root avulsion of C7, which is not clearly depicted on STIR or MR myelography images. Due to neurotmesis of several nerve roots, tractography was unable to depict continuous nerve structures lateral to the completely disconnected nerves.

4.4.4. Thoracic outlet syndrome

A further important indication for brachial plexus MRI is the detection of a compression or irritation of a plexus segment within the thoracic outlet, i.e., the presence of a neurogenic thoracic outlet syndrome. This type of involvement of the brachial plexus can be caused by a bone abnormality, such as a cervical rib, an elongated transverse process of C7 (Fig. 8), and a bony mass of the first rib or clavicle, or by a soft tissue abnormality, such as a fibrous band, muscle insertion, and volume abnormalities, as well as soft-tissue scaring and neoplasms. Plexus compression usually increases with elevation or sustained use of the arm due to a volume reduction in the interscalene triangle and the costoclavicular space, where the brachial plexus passes through. Therefore, to detect a plexus encroachment, the postural situation of the arm that provokes the clinical symptoms should be reproduced during MR imaging by means of a dynamic MR evaluation, i.e., first, MR imaging in the neutral position with the arm lying beside the body, and then, with the arm in a hyperabduction position [13]. This MR technique allows the depiction of the dynamic space reduction around the brachial plexus, as well as the displacement or compression of some parts of the plexus.

5. Microstructural evaluation of the brachial plexus

5.1. Diffusion-weighted imaging

Diffusion-weighted imaging (DWI) has been recently introduced as a noninvasive technique to visualize peripheral nerves, including the brachial plexus, because of its excellent suppression of background structures such as fat, muscles, and vascular structures [6]. The main advantage of DWI of the peripheral nerves, in general, and the brachial plexus, in particular, is its ability to differentiate and highlight the nerves over long trajectories from their surrounding structures, which may have similar signal intensities on conventional MR sequences. With DWI, it is possible to visualize the spinal cord, ganglia, postganglionic nerve roots, and peripheral nerves. However, the visualization of plexus nerve segments might be degraded by overprojection of normal structures that maintain
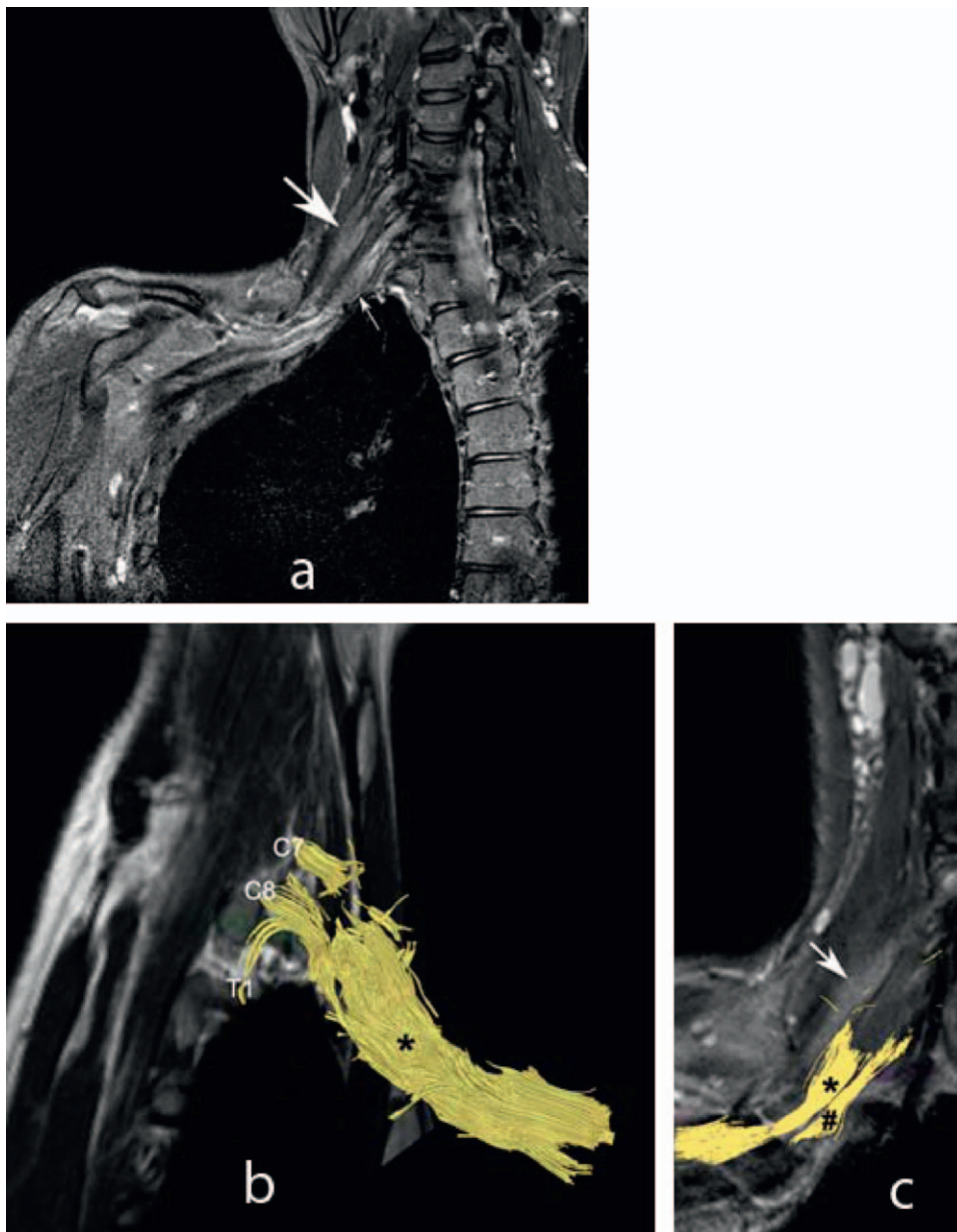
Fig. 11. A brachial plexus birth injury in a 24-year-old patient. (a) Paracoronal 2D T2 STIR shows a neuroma-in-continuity of the upper trunk (large arrow). In addition, the middle trunk (small arrow) and the cords (arrowheads) are diffusely thickened. (b) Paracoronal 3D tractogram shows a considerable mass-like accumulation (asterisk) of nerve fibers in the middle and lower trunks and their cords. No nerve fibers could be detected upwards of C7. (c) Paracoronal 2D tractogram superimposed on the respective paracoronal STIR image also shows no nerve fibers in the neuroma-in-continuity of the upper trunk, while multiple nerve fibers were detected in the middle (asterisk) and lower trunk (#). The tractograms suggest the presence of a second neuroma-in-continuity, with functional nerve fibers, and that the upper trunk contains no significantly operative nerve fibers. DTI and tractography revealed several disorganized trajectories within the neuroma, most probably reflecting the abnormal axonal arrangement within the posttraumatic nerve lesion.

high diffusion signal intensity, such as bone marrow and lymph nodes, and veins with slow blood flow.

5.2. Diffusion tensor imaging

DTI is a technique that was introduced in the early nineties [14,15], and has become, since then, a clinical imaging tool for imaging the peripheral nerves [16–18] and spinal cord [19]. DTI provides quantitative information about water diffusion within axons, depending on the different diffusion properties of water molecules according to their environment. In contrast to the isotropic diffusion of cerebrospinal fluid, with which water molecules have an equal range of motion in all directions, the diffusion of water molecules in the neural tracts of the white matter is anisotropic, i.e., the motion of water molecules in an axon is greater and faster in the direction of the axon's long axis than in any other direction. This principle is the basis of DTI and its main function is to record the anisotropy and orientation of the axons.

Accordingly, a perfectly isotropic diffusion voxel on a diffusion tensor image is assumed to be a sphere (since the range of motion of diffusion is equal in all directions), whereas the probabilistic shape of an anisotropic voxel is an ellipsoid consisting of three orthogonal vectors that each has a direction and an associated scalar magnitude. The magnitudes of the three vectors are called eigenvalues ($\lambda1$, $\lambda2$, $\lambda3$). The vector having the highest eigenvalue is the primary eigenvector, and represents the main direction of the ellip-
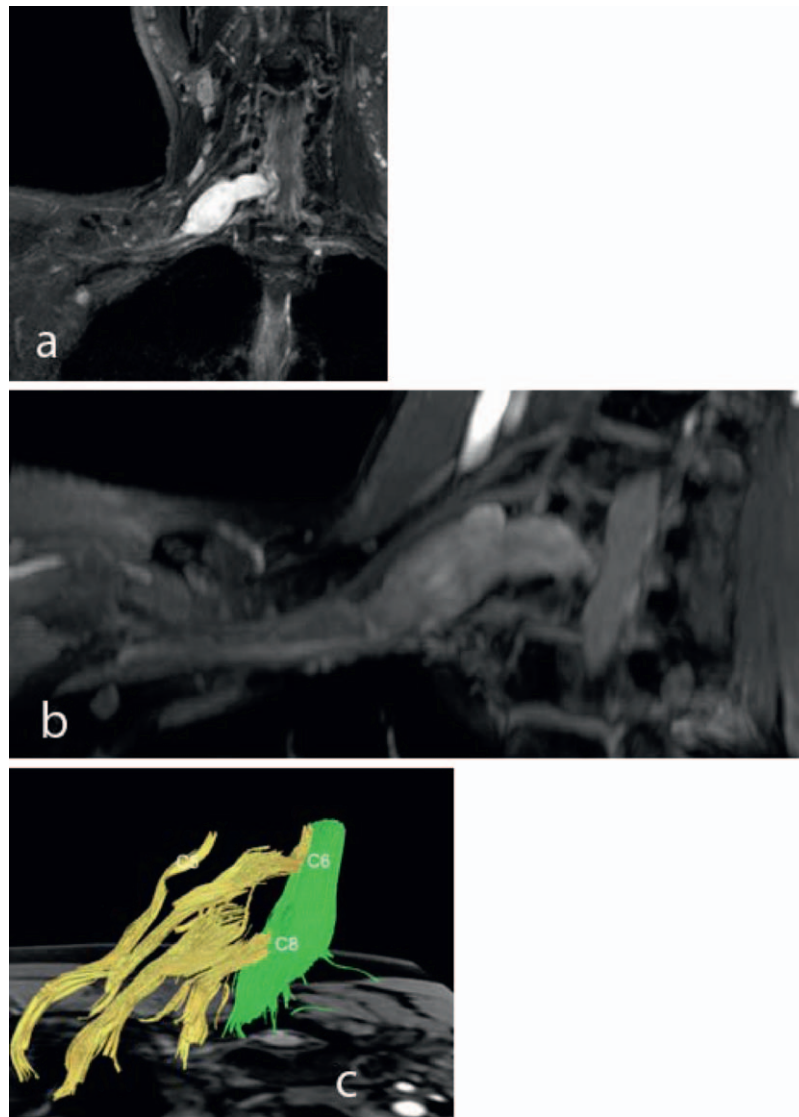
Fig. 12. Plexiform neurofibroma of C7 and the middle trunk in a patient with known neurofibromatosis 1. (a) Thin paracoronal MIP image acquired from the paracoronal 2D T2 STIR images shows a hyperintense fusiform mass of C7 and the middle trunk. The distal part of the middle trunk arises from the center of the mass. (b) Thin paracoronal MIP image acquired from the axial contrast-enhanced THRIVE images shows moderate and homogenous enhancement of the mass. (c) 3D tractogramm shows the decentralization of the fibers of the distal part of C7 and the loosening of the fibers of the proximal part of the middle trunk, suggesting an intraneural growth of the mass with corresponding difficulties at surgical resection. This plexiform neurofibroma was resected, with an end-to-side neuroanastomosis (C7 to C6). The fibers of the proximal part of C7 could not be detected.

soid. The average of three eigenvalues, which quantifies the average range of water molecule motion, represents the mean diffusivity. From these diffusion tensor parameters, a number of indices of anisotropy can be calculated and then transformed to be visualized on a 2D anisotropy map that represents a parametric image of the anisotropy value in each voxel. The anisotropy values range between 0 (pure isotropic diffusion) and 1 (pure anisotropic diffusion). The most commonly used indices are the relative anisotropy (RA) and fractional anisotropy (FA). Both methods provide information on how far the diffusion values in a particular direction in space differ from the mean diffusivity. The degree of anisotropy provides information about the white matter structures, and thus, changes in diffusivity, particularly in FA, are believed to be sensitive measures of the microstructural integrity of nerves.

DTI can be considered a technical optimization of the diffusion-weighted imaging (DWI), which, in white matter imaging, provides an image of the movement ability of water molecules in the white matter structures. Thus, DWI provides information about the integrity of the white matter, but limited information about

the direction of the diffusion of water molecules. DWI is measured through the acquisition of two images for each slice, i.e., a T2-weighted image with a low b-value ($b = 0\,\text{s/mm}^2$) and a diffusion image with a high b-value ($1000\,\text{s/mm}^2$; now standard for clinical applications), and these two diffusion images are then applied to estimate the apparent diffusion coefficient (ADC). These images contain scant directional information.

Otherwise, when the direction of the diffusion needs to be assessed, it is necessary to acquire diffusion images with a high b-value in at least six noncollinear directions in addition to one $b = 0\,\text{s/mm}^2$ T2-weighted image and thereby determine the diffusion tensor. For imaging the brachial plexus, it is necessary to use a b-value that is less than the conventional $b = 1000\,\text{s/mm}^2$ in brain DTI because of the small volume of the plexus nerves, and therefore, the limited signal intensity. This value may range from $b = 600\,\text{s/mm}^2$ to $b = 800\,\text{s/mm}^2$ for plexus DTI. Applying the diffusion gradients in more directions will enable a better SNR, which will lead to a more accurate calculation of the diffusion tensor parameters, such as fractional anisotropy (FA), mean diffusivity,
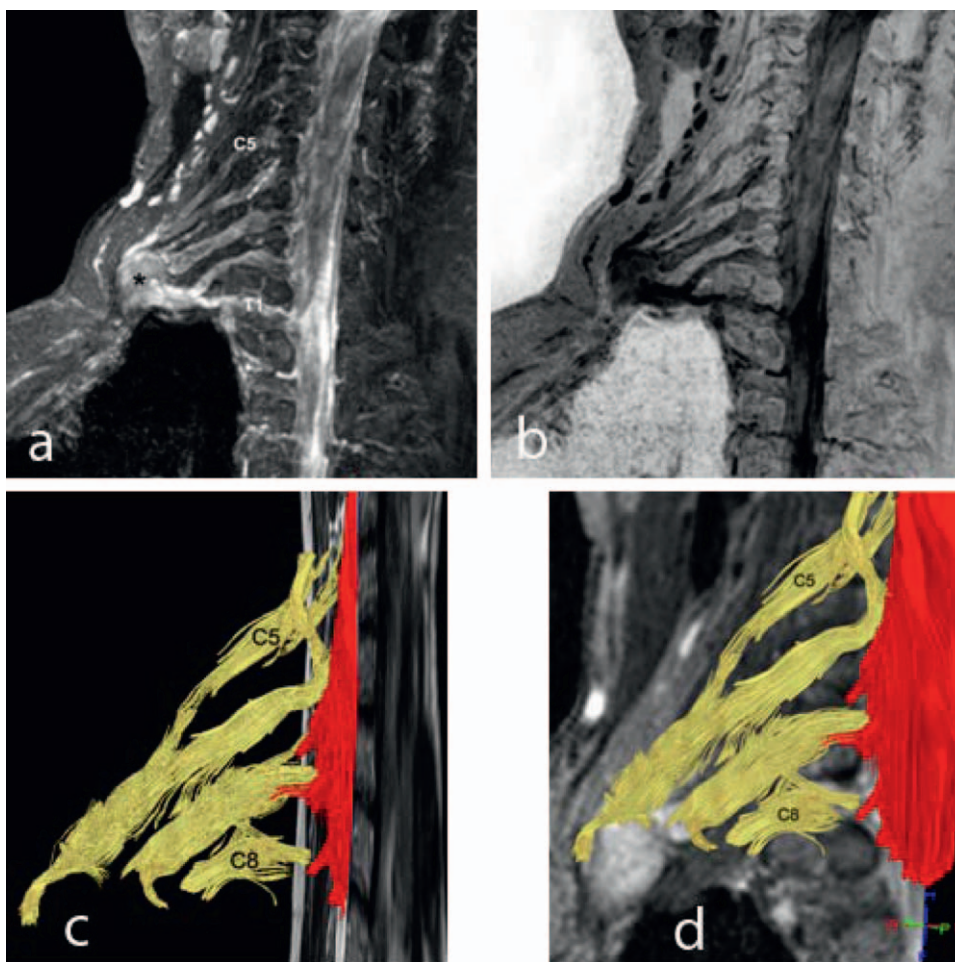
Fig. 13. Stump neuroma after interthoracoscapular (forequarter) amputation of the right upper extremity due to a highly malignant soft tissue tumor of the right axilla. (a) Thin MIP image acquired from the paracoronal 2D T2 STIR images and (b) thin inverted MIP image show all five roots of the brachial plexus and the proximal parts of the three trunks that end in a rounded mass (asterisk). (c) Paracoronal 3D tractogram and (d) paracoronal 3D tractogram superimposed on the STIR images show the nerve fibers intact from the spinal cord until they reach the neuroma, where the distal fibers of the upper and middle trunks are displaced and end around the neuroma. Due to the loss of the anisotropic nature of the lesioned nerve structures, no intact trajectories were visualized within the neuroma.

and eigenvalues [20]. However, the greater the gradient direction, the more time required and there is more risk for movement artifacts. Thus, a compromise is necessary between acquisition time and sample quality. A range of 16–40 gradient directions seems appropriate in clinical routine for robust estimation of the primary eigenvector, i.e., the tensor orientation. As a result, and depending on the determination of diffusion direction, DTI helps to evaluate the course of the white matter neural tracts. Another consideration in the imaging of the brachial plexus is the acquisition plane. The sagittal plane can be applied when only the right or left plexus needs to be evaluated, and the axial plane should be used when the central segments on both sides need to be evaluated.

5.3. Postprocessing

Leading MR vendors have provided DTI software, which allows for the easy and time-efficient postprocessing of DTI data. Generally, the applicability of this software in the assessment of the peripheral nervous system is similar to its use in the central nervous system. There are mainly two ways of interpreting DTI data in a qualitative way: one is the generation of fractional anisotropy (FA) color-coded maps; the other is the technique of tractography. FA color-coded maps visualize the orientation of anisotropy using a defined color for a certain diffusion orientation in space

(for instance: green – anteroposterior; blue – craniocaudal; red – left/right). Moreover, the brightness of a certain tissue region indicates the degree of anisotropy, reflected by the FA value (bright – high FA values, dark – low FA values). These maps can provide two-dimensional, semiquantitative information about the structure of an imaged nerve. Tractography, however, uses a tracking algorithm (generally and most frequently a linear tracking algorithm) in order to 3D depict tissue structures. Based on the fact that tissues, in general, do not show a certain uniformity in their anisotropy characteristics, it is necessary to define regions of interest *a priori*. By using pre-defined thresholds, the tracking algorithm will visualize the amount of "connectivity" by visualizing "fibers" or trajectories.

In DTI of the brachial plexus, both types of postprocessing can be helpful. FA color-coded maps demonstrate structures of high anisotropy and their 2D orientations – properties that generally apply to the peripheral nerves as well. After co-registering these maps with structural (T2-weighted, FLAIR, etc.) sequences, a template can be generated, which helps the examiner to identify regions of high anisotropy and localize them on structural sequences. For tractography, the ROIs are placed along a certain peripheral nerve (or nerve root) perpendicular to its orientation. Thus, all anisotropic structures that do not relate to peripheral nerve tissue can be excluded. This strategy avoids the inclusion of false-positive "trajectories" or "fibers" that mainly originate from the skeletal muscle.
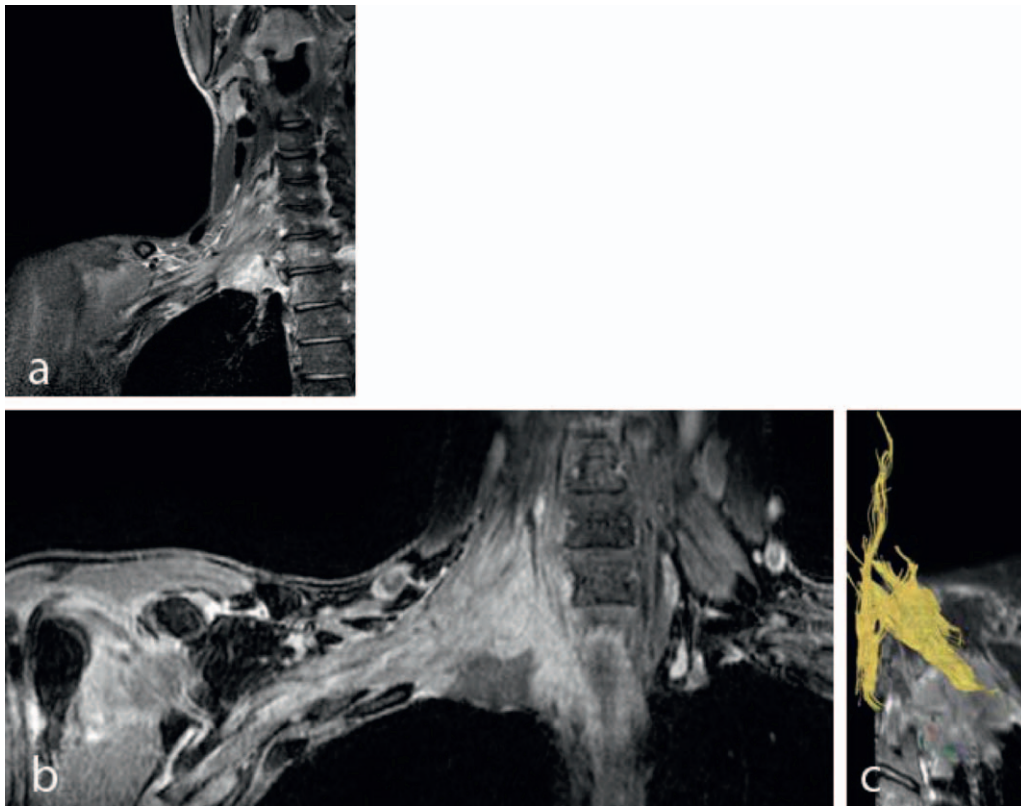
Fig. 14. Superior sulcus tumor (Pancoast tumor). (a) Paracoronal 2D T2 STIR image shows the Pancoast tumor infiltrating T1 and C8 and the distal part of C7, while C6 and C5 are thickened and severely hyperintense. (b) Coronal MPR image, reconstructed from the axial contrast-enhanced THRIVE images, shows the extent of the tumor surrounding all roots and trunks of the brachial plexus. (c) 3D tractogram showing considerable and well-arranged fibers of C5, C6 and the proximal part of the upper trunk until the trunk becomes encompassed by the Pancoast tumor. The fibers of the other plexus roots were not detected due tumor infiltration.

5.4. Tractography

The computer-aided 3D tract-tracking technique known as trac-tography is a DTI postprocessing technique, which allows the 3D visualization of tissue anisotropy by generating geometrical equiv-alents of water diffusion – called "trajectories" or fibers. Currently, most of the tractography algorithms available in the clinical setting are tract propagation techniques. These techniques use streamline tracking algorithms and a deterministic approach, with an *a priori* definition of specific anatomical landmarks (e.g., regions of inter-est or seed points), through which the generated trajectories are expected to pass. In addition to the *a priori* definition and knowl-edge of the "expected" result, different parameters, such as the minimum FA value of the studied trajectory, the maximum turn-ing angle, and the minimum fiber length, can be arbitrarily chosen by the examiner. Therefore, this technique is, to some extent, lim-ited by the lack of standardization. The postprocessing procedures of DTI are still time-consuming and limit the clinical application of this technique, particularly in a setting with a high workload. How-ever, the opportunity to visualize the complex diffusion patterns of certain tissue types in a 3D manner is a great advantage of this technique and is particularly worthwhile when imaging complex anatomical regions, such as the brachial plexus.

5.5. DTI with tractography in clinical practice

5.5.1. Trauma

The diagnosis of an acute or subacute traumatic injury of the brachial plexus is usually made on the structural imaging sequences. DTI with tractography enables the depiction of the plexus nerves fibers that are not detectable on conventional MR

imaging. Because of CSF flow artifacts DTI and tractography are cur-rently not suitable for the evaluation of the intradural rootlets of the brachial plexus, which remains confined to MR myelography sequences. However, DTI with tractography enables a perspective of the function and continuity of the extraforaminal plexus roots, which are also frequently involved in traumatic plexus injuries. A traumatic injury of a peripheral nerve can range from neurapraxia, a dysfunctional state of the axons, to axonotmesis and neurotmesis, where the plexus root is severely hampered and should preferably undergo surgical repair. Since the indication and success of sur-gical repair of lateral root avulsion injuries is dependent on the severity and extent of the lesion, a non-invasive technique, which may potentially differentiate between the different grades of nerve injury, would be extremely valuable. It is believed that DTI and trac-tography depict only peripheral nerves, which the majority of their axons is intact. Thus, the visualization of well-tractable and con-tinuous nerve fibers would rule-out a significant axonal damage of the plexus nerves (Fig. 9). On the contrary, the non-visualization of the entire or part of a nerve root on a DTI-tractogram would be related to the local disturbance of its diffusion characteristics indi-cating axonal damage, i.e., axonotmesis, or complete dissection, i.e., neurotmesis (Fig. 10). In general, DTI cannot detect the nerve fibers distal to the rupture site. However the validity of these assumptions must be subject to future research.

5.5.2. Tumors

The application of DTI with tractography on neoplastic lesions of the brachial plexus has been recently evaluated and was found to be feasible and helpful in several ways [17]. Since tractogra-phy provides a three-dimensional visualization of the plexus nerve roots, the spatial anatomical relationship of a primary benign or
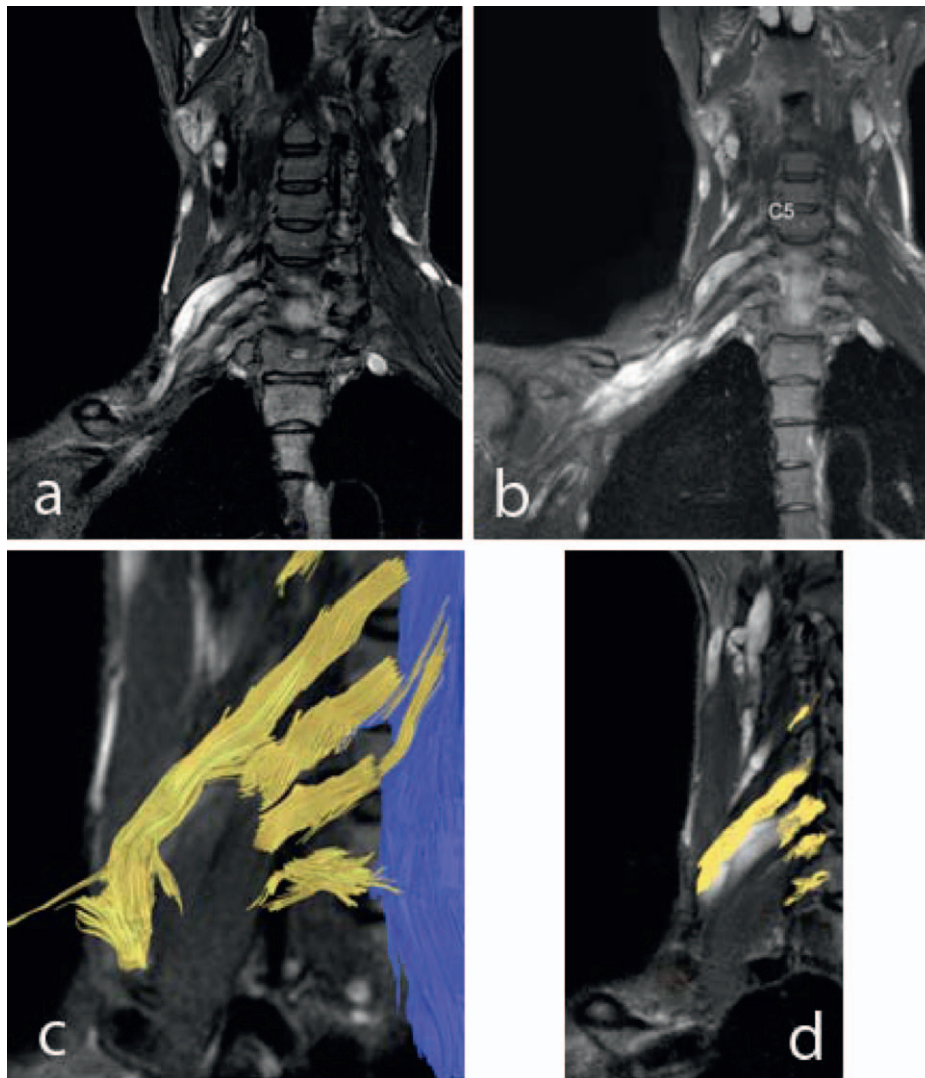
Fig. 15. Reconstruction of C5 with a sural nerve graft to the posterior cord in a patient with neurofibromatosis 1. (a) Paracoronal 2D T2 STIR and (b) thin paracoronal MIP image, acquired from the paracoronal 2D T2 STIR images, show the neurofibromas at C6, C8, and the plexus cords. C5 is not sufficiently demonstrated. (c) 3D tractogram and (d) 2D tractogram superimposed on the paracoronal STIR images show a patent spinal root at C5 and its transplanted nerve graft.
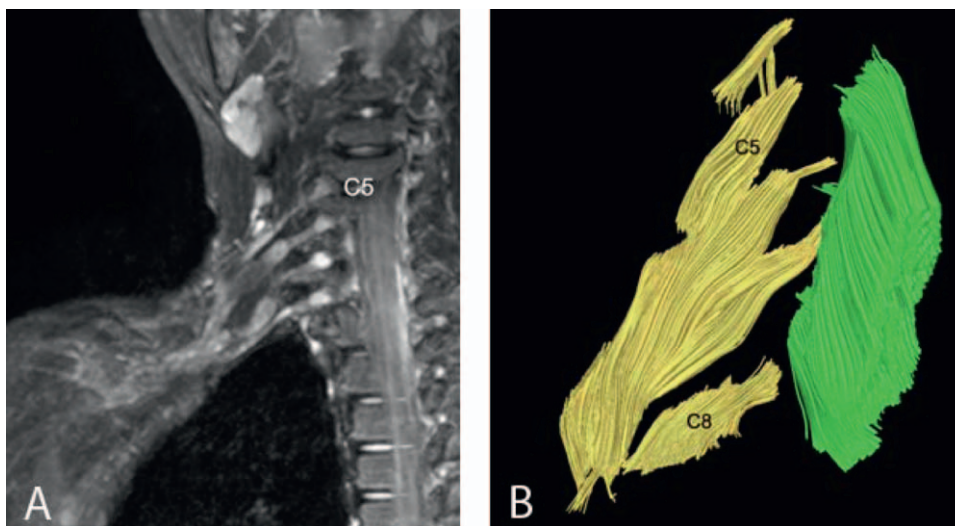

Fig. 16. Obstetric brachial plexus injury in an eight-year-old boy with neurolysis of C5, C6, and C7 as well as of the upper and middle trunk at the age of seven months. (a) Paracoronal thin MIP image acquired from the paracoronal 2D T2 STIR images shows a mild irregular form of C5 to C8 and moderate diffuse thickening of the upper and middle trunks. (b) Paracoronal 3D tractogram shows thickening of the brachial plexus neural structures; however, the nerve fibers could be well-recognized with no interruption or displacement.

malignant peripheral nerve sheet tumor involving the plexus roots can be evaluated. Thus, this technique may help to guide the surgical approach to these lesions. Further, tractography provides information about the nerve structure and orientation, including fiber disorganization (Fig. 11), displacement (Figs. 12 and 13), and destruction (Fig. 14). In general it is believed that benign tumors cause fiber disorganization or displacement and malignant tumors cause fiber destruction. Thus, according to the fibers character on a DTI-tractogram, a differential diagnosis of the plexus neoplastic lesion could be made. Moreover, tractography may allow the differentiation between some benign neurogenic tumors, i.e., neurofibroma and schwannoma. A neurofibroma causes usually a fusiform distention of the nerve with diffuse loosening of the nerve fibers (Fig. 12c). A schwannoma causes usually a spherical distention of the nerve with splitting of the nerve fibers, similar to that seen by a stump neuroma (Fig. 13c). In addition, DTI has the potential to identify peripheral nerve infiltration by malignant tumors, particularly Pancoast tumors, by the detection and quantification of abnormal peripheral nerve diffusion characteristics at the site of nerve root encasement. This may help to guide further oncological treatment strategies.

5.5.3. Postoperative follow-up

As in the assessment of axonal injury and Wallerian degeneration, DTI shows great potential as a non-invasive technique for the follow-up evaluation of peripheral nerve injuries and operations and to detect axonal regeneration, although there are very few studies on this subject. In a recent study assessing peripheral nerve regeneration, DTI indices were found to be useful in the detection of axonal regeneration after an injury and in the differentiation between the degenerative phase, which leads to decreased FA and increased radial diffusivity ($\lambda 2$, $\lambda 3$), and the regenerative phase, which leads to increased FA and decreased radial diffusivity [21]. Furthermore, DTI can be used to assess the axonal integrity of the brachial plexus roots after brachial plexus neurolysis or reconstruction with nerve transfer. After brachial plexus reconstruction, the presence of intact nerve fibers within the transferred nerve indicates vitality of the implant and patent function of the operated nerve root (Fig. 15). Similarly, in case of brachial plexus neurolysis, postoperative functional recovery of the operated plexus roots can be assumed when FA values are restored and the nerve fibers of the designated roots can be well-recognized with no interruption or displacement on tractography (Fig. 16).

6. Conclusions

3 T MR neurography can be a valuable method for the noninvasive evaluation of the brachial plexus. Diffusion tensor imaging with tractography can be combined with conventional plexus MR imaging to provide a comprehensive evaluation of the brachial plexus and its surrounding structures in patients with symptoms referable to the brachial plexus. The STIR, BTFE, and THRIVE sequences are excellent techniques for demonstrating structural disorders of the brachial plexus, whereas DTI with tractography provides a unique perspective about the microstructure and function of the white matter tracts of the brachial plexus, and assists in interpreting conventional MR images. In particular, DTI assists in the evaluation of neural integrity in patients with traumatic or neoplastic nerve disorders, as well as for the assessment of neural function recovery in patients after surgical treatment.

References

[1] Howe FA, Filler AG, Bell BA, Griffiths JR. Magnetic resonance neurography. Magn Reson Med 1992;28:328–38.
[2] Du R, Auguste KI, Chin CT, Engstrom JW, Weinstein PR. Magnetic resonance neurography for the evaluation of peripheral nerve, brachial plexus, and nerve root disorders. J Neurosurg 2010;112:362–71.
[3] van Es HW, Bollen TL, van Heesewijk HP. MRI of the brachial plexus: a pictorial review. Eur J Radiol 2010;74:391–402.
[4] Vargas MI, Viallon M, Nguyen D, Beaulieu JY, Delavelle J, Becker M. New approaches in imaging of the brachial plexus. Eur J Radiol 2010;74:403–10.
[5] Viallon M, Vargas MI, Jlassi H, Lovblad KO, Delavelle J. High-resolution and functional magnetic resonance imaging of the brachial plexus using an isotropic 3D T2 STIR (Short Term Inversion Recovery) SPACE sequence and diffusion tensor imaging. Eur Radiol 2008;18:1018–23.
[6] Takahara T, Kwee TC, Hendrikse J, et al. Subtraction of unidirectionally encoded images for suppression of heavily isotropic objects (SUSHI) for selective visualization of peripheral nerves. Neuroradiology 2010.
[7] Johnson EO, Vekris M, Demesticha T, Soucacos PN. Neuroanatomy of the brachial plexus: normal and variant anatomy of its formation. Surg Radiol Anat 2010;32:291–7.
[8] van den Brink JS, Watanabe Y, Kuhl CK, et al. Implications of SENSE MR in routine clinical practice. Eur J Radiol 2003;46:3–27.
[9] Tagliafico A, Succio G, Emanuele Neumaier C, et al. MR imaging of the brachial plexus: comparison between 1.5-T and 3-T MR imaging: preliminary experience. Skeletal Radiol 2010.
[10] Zhang Z, Song L, Meng Q, et al. Segmented echo planar MR imaging of the brachial plexus with inversion recovery magnetization preparation at 3.0 T. J Magn Reson Imaging 2008;28:440–4.
[11] Barth MM, Smith MP, Pedrosa I, Lenkinski RE, Rofsky NM. Body MR imaging at 3.0 T: understanding the opportunities and challenges. Radiographics 2007;27:1445–62, discussion 62–4.
[12] Okada T, Miki Y, Fushimi Y, et al. Diffusion-tensor fiber tractography: intraindividual comparison of 3.0-T and 1.5-T MR imaging. Radiology 2006;238:668–78.
[13] Demondion X, Herbinet P, Van Sint Jan S, Boutry N, Chantelot C, Cotten A. Imaging assessment of thoracic outlet syndrome. Radiographics 2006;26:1735–50.
[14] Le Bihan D, Breton E, Lallemand D, Grenier P, Cabanis E, Laval-Jeantet M. MR imaging of intravoxel incoherent motions: application to diffusion and perfusion in neurologic disorders. Radiology 1986;161:401–7.
[15] Basser PJ, Mattiello J, LeBihan D. Estimation of the effective self-diffusion tensor from the NMR spin echo. J Magn Reson B 1994;103:247–54.
[16] Andreisek G, White LM, Kassner A, Sussman MS. Evaluation of diffusion tensor imaging and fiber tractography of the median nerve: preliminary results on intrasubject variability and precision of measurements. AJR Am J Roentgenol 2010;194:W65–72.
[17] Vargas MI, Viallon M, Nguyen D, Delavelle J, Becker M. Diffusion tensor imaging (DTI) and tractography of the brachial plexus: feasibility and initial experience in neoplastic conditions. Neuroradiology 2010;52:237–45.
[18] Khalil C, Budzik JF, Kermarrec E, Balbi V, Le Thuc V, Cotten A. Tractography of peripheral nerves and skeletal muscles. Eur J Radiol 2010.
[19] Budzik JF, Balbi V, Le Thuc V, Duhamel A, Assaker R, Cotten A. Diffusion tensor imaging and fibre tracking in cervical spondylotic myelopathy. Eur Radiol 2011;21:426–33.
[20] Mukherjee P, Chung SW, Berman JI, Hess CP, Henry RG. Diffusion tensor MR imaging and fiber tractography: technical considerations. AJNR Am J Neuroradiol 2008;29:843–52.
[21] Morisaki S, Kawai Y, Umeda M, et al. In vivo assessment of peripheral nerve regeneration by diffusion tensor imaging. J Magn Reson Imaging 2011.